Optical manipulation of Rayleigh particles by metalenses: A numerical study

ZHE SHEN,[1,*] HONGCHAO LIU,[2] SHUANG ZHANG,[2] YAO-CHUN SHEN,[3] BAIFU ZHANG,[1] AND SAIYU LUO[1]

[1]*School of Electronics Engineering and Opto-electronic Technology, Nanjing University of Science and Technology, Nanjing 210094, China*
[2]*School of Physics & Astronomy, University of Birmingham, Birmingham B15 2TT, UK*
[3]*Department of Electrical Engineering & Electronics, University of Liverpool, Liverpool L69 3GJ, UK*
**shenzhe@njust.edu.cn*

Abstract: Based on the focusing feature of metalens, we numerically studied its application in optical manipulation of Rayleigh particles. Three types of metalens: point-focusing, line-focusing and line-focusing with phase gradient were designed. Simulation results using Finite-Difference Time-Domain (FDTD) method showed that the incident optical beams can be focused into a spot or a line for stable particles trapping. Through engineering a gradient phase in the direction of the focal line, the proposed metalens can push the particles along the line. This provides a unique capability to move particles along a line without the need of any mechanical movement. Given its thin sheet structure and compactness, the proposed metalens can be easily integrated into microfluidic and optical tweezers systems, and it can find potential applications in optical sorting of biological cells.

1. Introduction

Optical tweezers, invented by Ashkin *et al.* in 1986, utilize a highly focused laser beam to trap particles [1]. Due to its noninvasive advantage, optical tweezers have been widely used in life science, diagnostics, and analytical chemistry. To generate the highly focused laser beam, conventional optical tweezers system requires high Numerical Aperture (NA) objective lens, which is bulky and expensive. Also, it is a challenging task to assemble this kind of complex and bulk optics into a tiny chip at low cost for integrating the optical trapping and sorting systems, thus there is a need to develop new focusing mechanisms and lenses to meet current trends of instrument integration and miniaturization. Along with the requirement of portable and convenient analysis and diagnostics, lab-on-a-chip and optofluidic devices are becoming an emerging target of research.

In the recent two decades, waveguide configuration has promoted the development of integrated trapping system, which was initiated in 1996 by Kawata *et al.* with the work that Mie particles were optically propelled in a channeled waveguide [2]. This configuration allows easy separation of the propagating path of the light from the motion path of the propelled particles. Particles located at the vicinity of the surface can be driven through a short distance because an evanescent field is generated and localized on the surface. Generally, optical force of a particle depends on properties such as refractive index and size of the particle. This characteristic can be applied for particle or biological cell sorting [3]. A variety of structures such as Y-branched waveguide [4] have been exploited for demonstrating this application.

However, waveguide configuration has three main drawbacks. Firstly, there are scattering and absorption losses in waveguide, thus only a small portion of total transport light can be coupled to evanescent field. This inefficient coupling configuration requires large laser power to achieve good interaction distance between the evanescent field and the particle. Secondly, due to the nature of the evanescent field, the particle solution would inevitably have physical contact with the waveguide in the trapping process. This may lead to potential contamination

of the waveguide after a single use, limiting its usage in multiple measurements. Thirdly, only propulsion of particles can be obtained in the channeled waveguide. In order to trap particles, one needs to achieve high optical intensities in the waveguide by introducing resonant structures such as whispering gallery mode resonator [5] and micro-ring resonator [6], but particles cannot be trapped at specific areas. Further applications through integrating optical tweezers system with waveguide configuration would be hampered by these drawbacks.

Developing more integratable configuration to manipulate light with more degrees of freedom is highly demanded. In the last decade, metasurfaces, a new class of metamaterials that consist of planar subwavelength structures atop dielectric substrate have shown excellent flexibility for manipulating the phase, amplitude, polarization and angular momentum of light [7]. Due to its property of shaping wavefronts, metasurfaces have been used to demonstrate various applications including metalens [8-11], metasurface holograms [12-14], metasurface quarter-wave plate [15], and polarization converter [7]. In particular, metalens has provided a new solution to the integrated optical trapping application.

Metalens configuration can overcome the drawbacks of the waveguide configuration. Like objective configuration, it can focus light efficiently thus the laser power can be utilized fully for trapping. Meanwhile, it keeps the advantage of noninvasiveness. In addition, metalens can be designed for arbitrarily manipulating the focal field, where particles not merely experience pushing force.

In this paper, we propose an application of metalens for optical trapping and investigate three basic types of metalenses. Optical forces and trapping potentials were calculated to analyze the behaviors of particles in the focal fields by these three metalenses. Simulation results demonstrate that metalens is a versatile structure for optical manipulation of particles.

2. Methods and theory

2.1 The metalens structure

Figure 1(a) shows a schematic of a transmissive dielectric metalens. The basic unit of the metalens is a transparent Si nanofin [Fig. 1(b)]. To function like a spherical lens, the phase profile $\varphi(x, y)$ of the metalens needs to follow [16]

$$\varphi(x, y) = \frac{2\pi}{\lambda}(f - \sqrt{x^2 + y^2 + f^2}), \tag{1}$$

where λ is the design wavelength, x and y are the coordinates of each nanofin, and f is the focal length. It is crucial that the phase change for the incident and transmitted light can be altered smoothly from 0 to 2π. Due to the structural birefringence, the effective refractive index of the nanofin would be different for two orthogonal polarizations normal to the propagation direction. The individual orientation angle of a given nanofin, with respect to the *x*-axis, controls the abrupt phase change of the cross-CP (circularly polarized) scattered light. This phase profile is imparted via rotation of each nanofin at a given coordinate (x, y) by an angle, which is between the long axis of the nanofin and the *x* axis. In the case of right-handed circularly polarized incident light, these rotations yield a Pancharatnam Berry (PB) phase [17, 18], $\varphi(x, y) = 2\theta(x, y)$, accompanied by polarization conversion to left-handed circularly polarized light. Thus, each nanofin at (x, y) is rotated by an angle

$$\theta(x, y) = \frac{\pi}{\lambda}(f - \sqrt{x^2 + y^2 + f^2}). \tag{2}$$

To maximize the polarization conversion efficiency, the nanofins should operate as half waveplates. This is achieved due to the birefringence arising from the asymmetric cross section of nanofins with appropriately designed height, width, and length. These parameters can be optimized with using a three dimensional (3D) electromagnetic field simulation software (CST

Studio Suite). By choosing the nanofin with length, width and thickness of 300 nm, 180 nm and 500 nm, respectively, as shown in Fig. 1(b), its functionality is designed to be a half-wave plate working at 1064 nm. Simulations show that conversion efficiency as high as 92.5% is achieved [Fig. 1(c)]. The conversion efficiency is calculated as the ratio of transmitted optical power with opposite helicity to the total incident power. Consequently, the nanofin is capable of significantly decreasing the background interference and increasing the purity of desired cross-CP light. In this way, metalens can be designed for a desired wavelength via tuning of the nanofin parameters.

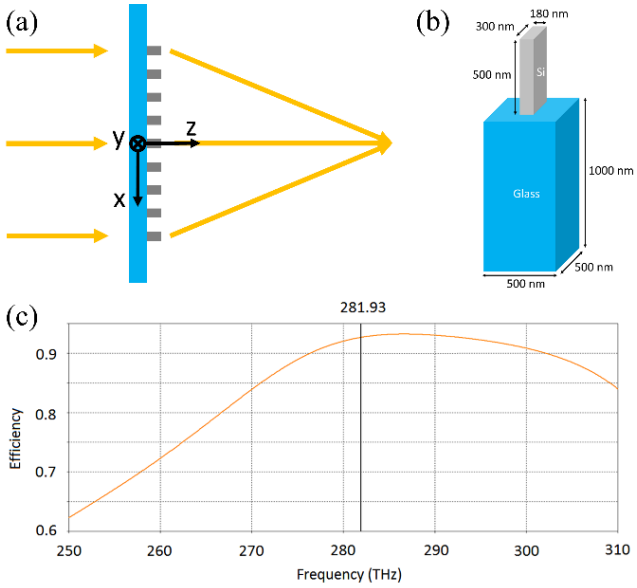

Fig. 1. (a) Schematic of the metalens. (b) The metalens unit consists of a Si nanofin supported by glass substrate. The dielectric constant of Si is 11.9. The refractive index of glass is 1.48. The centre-to-centre spacing of nanofins of metalens is 500 nm. (c) The transmittance efficiency through the metalens from left circular polarization to right circular polarization.

2.2 Optical force of Rayleigh particle and trapping potential

When the particle size is much smaller than the wavelength of the incident laser ($r \ll \lambda$), the particle is called Rayleigh particle, the force can be calculated by treating the particle as a dipole. The gradient force and scattering force can be readily separated with this approximation. Since calculating optical forces of particles is a scalar problem, means of ordinary diffractive optics was used [19]. For a sphere with radius r , the gradient force arises from the interaction between the induced dipole with the inhomogeneous field (E) as [20]

$$\boldsymbol{F}_{\text{grad}} = \pi n_{\text{m}}{}^2 \varepsilon_0 r^3 \left(\frac{m^2 - 1}{m^2 + 2} \right) \nabla |E|^2 , \tag{3}$$

where n_m is the refractive index of the medium, ε_0 the vacuum permittivity, m (n_p / n_m) the ratio of the refractive index of the sphere (n_p) to the refractive index of the medium (n_m). Since the scattering of Raleigh particle is weak, the scattering force hindering the trapping is negligible, we take the gradient force as the total force for Raleigh particle in following analysis.

Trapping potential can be calculated by the following formula [21]

$$U(r_0) = \int_{\infty}^{r_0} \mathbf{F}(r) \cdot d\mathbf{r} , \tag{4}$$

where $U(r_0)$ is the required energy to move the particle from the trap to infinity. Generally, in order to obtain a stable trap, more than 10 $k_B T$ trapping potential depth is needed to overcome the disturbance from the thermal effect [22], where k_B is the Boltzmann constant and T is the temperature.

3. Results and discussion

3.1 Optical trapping of Rayleigh particle by point-focusing metalens

The metalens used in Fig. 2 has a designed focal length of 5 μm and an aperture $5.5 \times 5.5\ \mu m^2$, consisting of 11 nanofins along the x and y directions with centre-to-centre separation of 500 nm. The rotation angles of the nanofins satisfy Eq. (2). The rotation angles for the nanofins far from the lens centre change more rapidly than those near the centre. This metalens can be fabricated by Electron-Beam Lithography (EBL) technique [16]. The NA is defined as $NA = n_s \sin[\tan^{-1}(D/2f)]$, where D is the diameter of the sub-lens, and n_s is the refractive index of the surrounding medium (water, $n_s = 1.33$) in the focal region. Consequently, the NA of the metalens is about 1.29, and the NA of the metalens can be further increased by introducing more 2π periods, giving rise to better focusing properties such as smaller focal spot size and stronger focal field.

By illuminating the metalens with right-hand circularly polarized light, the metalens functions as a converging (positive) lens, with the intensity profile of the focal field in the transverse plane (z = 5 μm) is shown in Fig. 2(a). The metalens causes the incident laser beam to converge at a focal plane on the transmission side of the lens forming a real focal spot. Thus, by manipulating the phase distribution along an interface with a suitably designed nanofin array for the incident circularly polarized light, a light wave can be fully concentrated. The Full Width at Half Maximum (FWHM) of the focal spot is approximately to be half wavelength, revealing the good focusing performance of the proposed metalens. Figure 2(c) shows the electric field in the transmissive y-z plane. The simulated focal plane is at about z = 4.27 μm, which is slightly different from the designed value. The focal depth is about 2 μm long, so this structure has potential to be used for generating Photonic Nanojet (PNJ).

The behavior of a particle within a focal region would depend on the induced optical force and related trapping potential. In all the simulations, the electric intensity of the incident field is normalized to 1 V/m. The incident optical power can be calculated by the following equation: $P = IS = \frac{cn\varepsilon_0}{2}|E|^2 S$, where I is the optical intensity, S the projected source area corresponding to the metalens area, c the speed of light in vacuum, n the refractive index of air, E the electric field. Both the trapping force F and the trapping potential U are proportional to the optical power P. In order to investigate the movement tendency of a Rayleigh particle, we calculated the force of the particle within the focal field. As shown in Fig. 2(b), the forces are all pointed towards the centre, especially in the area of focus spot. This proves the particle can be trapped in the focal plane. In the y-z plane as shown in Fig. 2(d), the majority of forces are pointed towards the focal spot. Therefore, 3D trapping can be performed with the focal field by the point-focusing metalens.

In order to study the stability of the trapping, trapping potential of a silica nanoparticle of a radius 100 nm in the focal field was calculated. The refractive index of the silica nanoparticle is 1.45. The temperature T is taken to be 298 K in all calculations. Clear trapping potential wells can be seen in Figs. 2(c) and (d), and they appear symmetrical. The barriers in x- and y-directions are located at $x = \pm 1.18\ \mu m$ and $y = \pm 1.25\ \mu m$, respectively. The lowest trapping potentials in x- and y- direction are both located at the centres, thus the particles have the tendency to move towards the focus centre. The calculations have considered the incident optical power. The depths of trapping potential wells in x- and y- directions are 6.59 $k_B T/\mu w$

and 5.67 $k_BT/\mu w$, respectively. Therefore, particles can be stably confined within the centre if the power of the incident light is more than 1.76 μw.

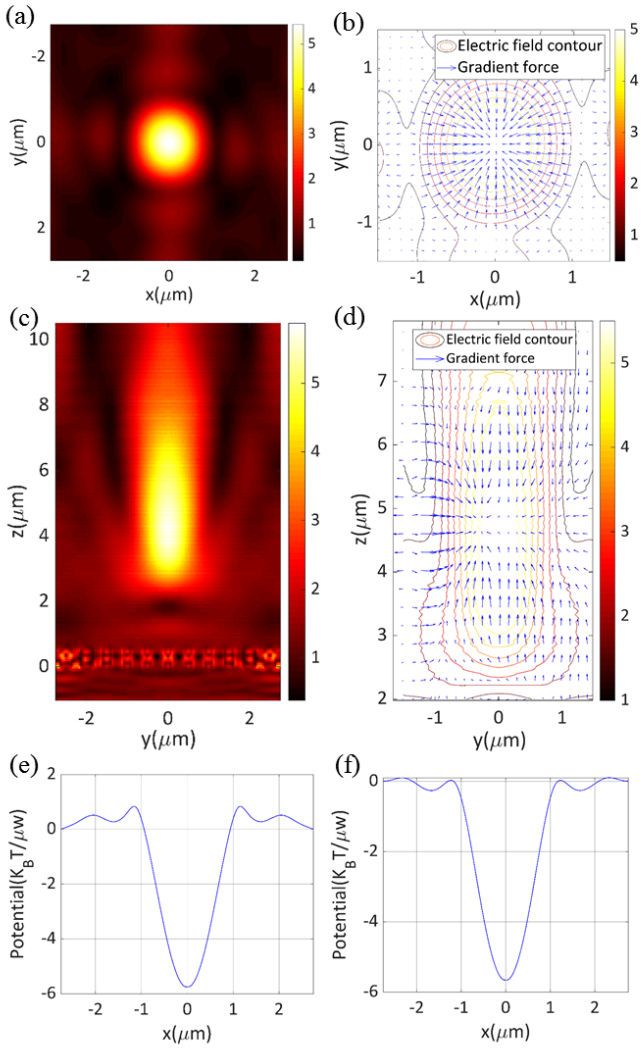

Fig. 2. The calculated focal fields, optical forces and trapping potentials by point-focusing metalens. (a) The electric field in the focal *x*-*y* plane. (b) The force distribution in the focal *x*-*y* plane. (c) The electric field in the longitudinal *y*-*z* plane. The dentoid pattern at $z = 0$ μm indicates the metalens. (d) The force distribution in the longitudinal *y*-*z* plane. (e) The trapping potential in *x* direction. (f) The trapping potential in *y* direction.

3.2 Optical trapping of Rayleigh particles by line-focusing metalens

To function like a line-focusing metalens (cylindrical metalens), the phase profile $\varphi(x, y)$ of the metalens needs to follow [23]

$$\varphi(x,y) = \frac{2\pi}{\lambda}(f - \sqrt{x^2 + f^2}), \tag{5}$$

where λ is the design wavelength, x and y are the coordinates of each nanofin, and f is the focal length. Each nanofin at (x, y) is rotated by an angle

$$\theta(x,y)=\frac{\pi}{\lambda}(f-\sqrt{x^2+f^2}). \tag{6}$$

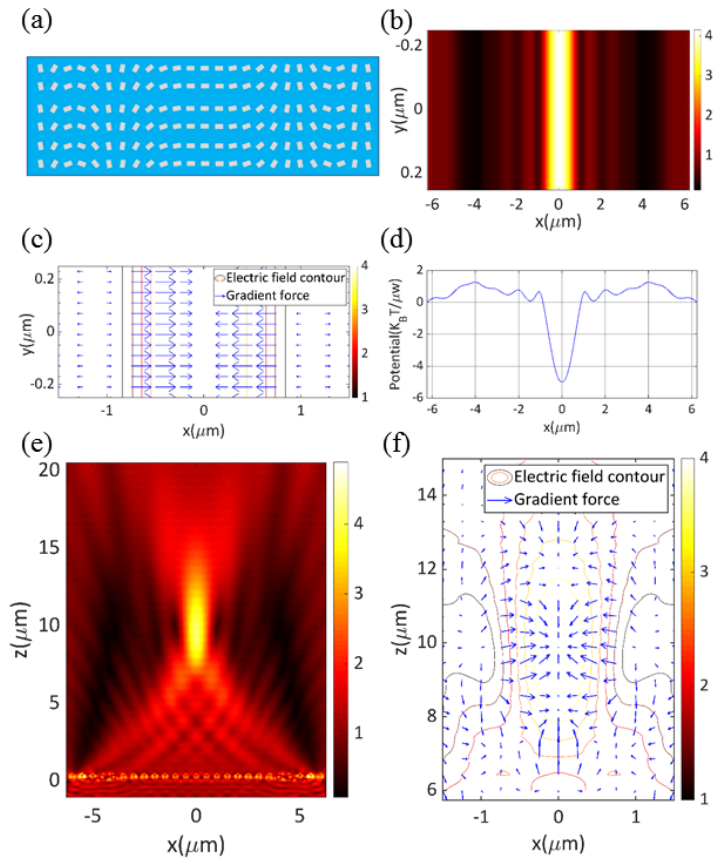

Fig. 3. (a) The nanofins pattern of the line-focusing metalens. The white rectangles indicate the nanofins, the blue background indicates the substrate, which is 12.5 μm long and 3 μm wide. (b) The electric field in the focal *x*-*y* plane. (c) The force distribution in the focal *x*-*y* plane. (d) The trapping potential in *x* direction. (e) The electric field in the longitudinal *x*-*z* plane. The dentoid pattern at $z = 0$ μm indicates the line-focusing metalens. (f) The force distribution in the longitudinal *x*-*z* plane.

The simulated lens in Fig. 3 has a designed focal length of 10 μm and an aperture $12.5\times3\ \mu m^2$, consisting of 6-row and 25-colomn nanofins with centre-to-centre space 500 nm, as shown in Fig. 3(a). As expected, the incident circularly polarized light is converged to a line in the middle of the plane at z =10 μm [Fig. 3(b)]. According to Eq. (3), we calculate the forces of Raleigh particles in the field of the focal plane. Almost all forces are pointed to the middle (x = 0 μm), as shown in Fig. 3(c), thus particles are pushed to the middle. In order to demonstrate the trapping stability, we calculated the trapping potential according to Eq. (4), a clear potential well can be seen as shown in Fig. 3(d). The depth of trapping potential well is 5.64 $k_BT/\mu w$. Therefore, 1.77 μw power incident light can maintain stable confinement of particles the focal line. This has potential applications in micro- control and assembly.

3.3 Optical manipulation of Rayleigh particles by line-focusing metalens with phase gradient

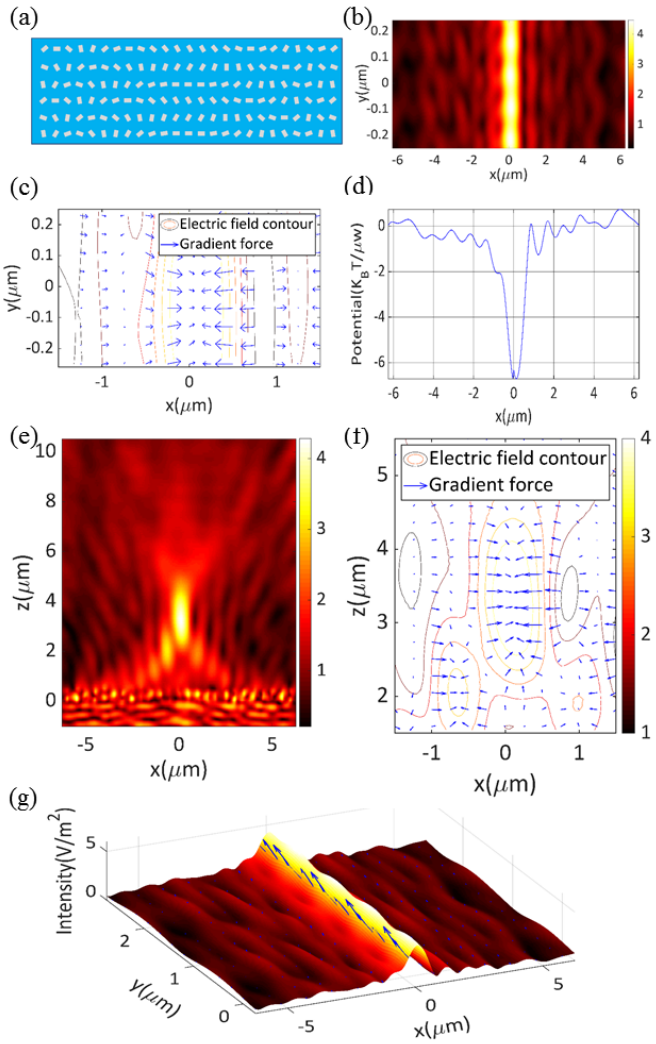

Fig. 4. (a) The nanofins pattern of line-focusing metalens with phase gradient in *y* direction. The white rectangles indicate the nanofins. The blue background indicates the substrate, which is 12.5 μm long and 3 μm wide. (b) The electric field in the focal *x*-*y* plane. (c) The force distribution in the focal *x*-*y* plane. (d) The trapping potential in *x* direction. (e) The electric field in the longitudinal *x*-*z* plane. (f) The force distribution in the focal *x*-*z* plane particle. (g) The Poynting vectors in the focal *x*-*y* plane. The blue arrows indicate the Poynting vectors.

In order to perform dynamic trapping with metalens, we add a gradient in *y* direction based on the structure of Fig. 3(a). As shown in Fig. 4(a), the first line at bottom is the same as that in Fig. 3(a), the rotation angles of nanofins increase by a step of π/3 from bottom to top. This additional phase can be expressed as

$$\theta(x,y)=\frac{\pi}{\lambda}(f-\sqrt{x^2+f^2})+\frac{\pi}{3d}y\,, \tag{7}$$

where d is the centre-to-centre spacing of nanofins. The phase profile $\varphi(x,y)$ of the metalens follows

$$\varphi(x,y)=\frac{2\pi}{\lambda}(f-\sqrt{x^2+f^2})+\frac{2\pi}{3d}y\,. \tag{8}$$

Figure 4(b) shows the electric intensity at the focal plane (z = 3.2 μm), demonstrating that a clear focusing line is formed. The gradient phase in y direction does not affect the focusing in x direction. Figure 4(c) shows the optical forces of Rayleigh particle in the focal area. The majority of the forces are pointed to the central line, and the central forces dominate. Figure 4(d) shows the potential well represented by the trapping potential along x direction. The depths of trapping potentials for the left and right barriers of the well are 6.11 $k_BT/\mu w$ and 6.83 $k_BT/\mu w$, respectively, implying that 1.64 μw laser power can maintain a robust trapping. The local minima of the trapping wells at both sides of the central well are not deep enough to confine a particle, thus particles are potentially trapped at the central line. Figure 4(e) shows the electric field distribution in the x-z plane (y =0 μm), where a clear focus spot can be seen. Figure 4(f) shows the forces experienced by the particle at each point of the x-z plane field, which shows that the particle has the tendency to move to the focus spot. Therefore, the focal field through the structure in Fig. 4(a) can still perform a 3D trapping.

Fig. 4(g) shows the Poynting vectors of the focal field in x-y plane. A clear energy flux can be seen along the line of x = 0 μm. The values of the Poynting vectors in other areas are much smaller. Since the scattering force is directed along the Poynting vector, particle would experience scattering force in the same direction. Therefore, particles trapped at the middle would be pushed along y+ direction, where phase gradient is applied. It is expected that particles especially high scattering or absorption particle such as metal particles would be pushed along the trajectory with gradient phase. This property is unique and different from that of traditional optical tweezers by objective, optical manipulation with evanescent wave and surface plasmon polaritons (SPPs). For optical manipulation by objective, the movement of particle relies on the movement of the particle solution or the focusing laser. For optical manipulation with evanescent wave and SPPs, the movement of particle is performed on the surface. This is a two-dimensional manipulation, and the movement distance is limited due to the decaying near-field. For our method, through line-focusing metalens with phase gradient, the captured particle can move along the line. Base on this method, through manipulating the focal field with designing metalens, 3D manipulation of particle can be achieved without the need of any mechanical movement. This has potential applications in drug delivery and optical sorting. The latter will be discussed in our next work. Moreover, our structure can be integrated with microfluidics chip, thus it provides a platform for potential application in biomedicine.

4. Conclusion

In summary, we numerically studied three types of metalenses: point-focusing, line-focusing and line-focusing with phase gradient, and they are capable of manipulating Rayleigh particles. The interaction between the focal fields and the nanoparticles was investigated with FDTD algorithm, and the induced mechanical effect was studied using analytical method. Our numerical simulations have shown for the first time that nanoparticles can not only be trapped into a line but also be moved along the trapping line by using line-focusing metalens with phase gradient. It is worth noting that the proposed metalens is within the fabrication capability of the concurrent nanofabrication techniques [16]. This dielectric flat lens opens an avenue for new applications of phase discontinuity devices, and could also have an impact on integrated photonic devices. This versatile trapping method may open up new avenues for optical tweezers and its application in biomedicine.

5. Funding and acknowledgments

5.1 Funding

Natural National Science Foundation of China (NSFC) (61604073, 61805119). National Science Foundation of Jiangsu Province (BK20160839, BK20180469, BK20180460).

Reference

1. A. Ashkin, J. M. Dziedzic, J. E. Bjorkholm, and S. Chu, "Observation of a single-beam gradient force optical trap for dielectric particles," Opt Lett **11**, 288-290 (1986).
2. S. Kawata, and T. Tani, "Optically driven Mie particles in an evanescent field along a channeled waveguide," Opt Lett **21**, 1768-1770 (1996).
3. X. C. Yuan, S. W. Zhu, J. Bu, Y. Y. Sun, J. Lin, and B. Z. Gao, "Large-angular separation of particles induced by cascaded deflection angles in optical sorting," Appl Phys Lett **93** (2008).
4. K. Grujic, O. G. Helleso, J. P. Hole, and J. S. Wilkinson, "Sorting of polystyrene microspheres using a Y-branched optical waveguide," Opt Express **13**, 1-7 (2005).
5. B. S. Schmidt, A. H. J. Yang, D. Erickson, and M. Lipson, "Optofluidic trapping and transport on solid core waveguides within a microfluidic device," Opt Express **15**, 14322-14334 (2007).
6. A. H. J. Yang, and D. Erickson, "Optofluidic ring resonator switch for optical particle transport," Lab Chip **10**, 769-774 (2010).
7. H. T. Chen, A. J. Taylor, and N. F. Yu, "A review of metasurfaces: physics and applications," Rep Prog Phys **79** (2016).
8. D. L. Lu, and Z. W. Liu, "Hyperlenses and metalenses for far-field super-resolution imaging," Nat Commun **3** (2012).
9. F. Aieta, P. Genevet, M. A. Kats, N. Yu, R. Blanchard, Z. Gaburro, and F. Capasso, "Aberration-Free Ultrathin Flat Lenses and Axicons at Telecom Wavelengths Based on Plasmonic Metasurfaces," Nano Lett **12**, 4932-4936 (2012).
10. B. Memarzadeh, and H. Mosallaei, "Array of planar plasmonic scatterers functioning as light concentrator," Opt Lett **36**, 2569-2571 (2011).
11. X. Ni, S. Ishii, A. V. Kildishev, and V. M. Shalaev, "Ultra-thin, planar, Babinet-inverted plasmonic metalenses," Light Sci Appl **2**, e72 (2013).
12. B. Walther, C. Helgert, C. Rockstuhl, F. Setzpfandt, F. Eilenberger, E.-B. Kley, F. Lederer, A. Tünnermann, and T. Pertsch, "Spatial and Spectral Light Shaping with Metamaterials," Adv Mater **24**, 6300-6304 (2012).
13. X. J. Ni, A. V. Kildishev, and V. M. Shalaev, "Metasurface holograms for visible light," Nat Commun **4** (2013).
14. G. Zheng, H. Mühlenbernd, M. Kenney, G. Li, T. Zentgraf, and S. Zhang, "Metasurface holograms reaching 80% efficiency," Nat Nano **10**, 308-312 (2015).
15. N. Yu, F. Aieta, P. Genevet, M. A. Kats, Z. Gaburro, and F. Capasso, "A Broadband, Background-Free Quarter-Wave Plate Based on Plasmonic Metasurfaces," Nano Lett **12**, 6328-6333 (2012).
16. M. Khorasaninejad, W. T. Chen, R. C. Devlin, J. Oh, A. Y. Zhu, and F. Capasso, "Metalenses at visible wavelengths: Diffraction-limited focusing and subwavelength resolution imaging," Science **352**, 1190-1194 (2016).
17. M. V. Berry, "The Adiabatic Phase and Pancharatnam's Phase for Polarized Light," J Mod Optic **34**, 1401-1407 (1987).
18. S. Pancharatnam, "Generalized theory of interference, and its applications," Proceedings of the Indian Academy of Sciences - Section A **44**, 247-262 (1956).
19. J. Liesener, M. Reicherter, T. Haist, and H. J. Tiziani, "Multi-functional optical tweezers using computer-generated holograms," Opt Commun **185**, 77-82 (2000).
20. Y. Harada, and T. Asakura, "Radiation forces on a dielectric sphere in the Rayleigh scattering regime," Opt Commun **124**, 529-541 (1996).
21. L. Novotny, R. X. Bian, and X. S. Xie, "Theory of nanometric optical tweezers," Phys Rev Lett **79**, 645-648 (1997).
22. A. H. J. Yang, T. Lerdsuchatawanich, and D. Erickson, "Forces and Transport Velocities for a Particle in a Slot Waveguide," Nano Lett **9**, 1182-1188 (2009).
23. X. Z. Chen, L. L. Huang, H. Muhlenbernd, G. X. Li, B. F. Bai, Q. F. Tan, G. F. Jin, C. W. Qiu, S. Zhang, and T. Zentgraf, "Dual-polarity plasmonic metalens for visible light," Nat Commun **3** (2012).